

# Distributed Activity Detection for Cell-Free Hybrid Near-Far Field Communications

Jingren Lei<sup>\*†</sup>, Yang Li<sup>†</sup>, Zeyi Ren<sup>\*</sup>, Qingfeng Lin<sup>\*</sup>, Ziyue Wang<sup>‡</sup>, Ya-Feng Liu<sup>§</sup>, and Yik-Chung Wu<sup>\*</sup>

<sup>\*</sup>Department of Electrical and Electronic Engineering, The University of Hong Kong, Hong Kong

<sup>†</sup>School of Computing and Information Technology, Great Bay University, Dongguan, China

<sup>‡</sup>LSEC, ICMSEC, AMSS, Chinese Academy of Sciences, Beijing, China

<sup>§</sup> School of Mathematical Sciences, Beijing University of Posts and Telecommunications, Beijing, China

Emails: {lei jr, renzeyi, qflin, ycwu}@eee.hku.hk, liyang@gbu.edu.cn, ziyuewang@lsec.cc.ac.cn, yafengliu@bupt.edu.cn

**Abstract**—A great amount of endeavor has recently been devoted to activity detection for massive machine-type communications in cell-free massive MIMO. However, in practice, as the number of antennas at the access points (APs) increases, the Rayleigh distance that separates the near-field and far-field regions also expands, rendering the conventional assumption of far-field propagation alone impractical. To address this challenge, this paper considers a hybrid near-far field activity detection in cell-free massive MIMO, and establishes a covariance-based formulation, which facilitates the development of a distributed algorithm to alleviate the computational burden at the central processing unit (CPU). Specifically, each AP performs local activity detection for the devices and then transmits the detection result to the CPU for further processing. In particular, a novel coordinate descent algorithm based on the Sherman-Morrison-Woodbury update with Taylor expansion is proposed to handle the local detection problem at each AP. Moreover, we theoretically analyze how the hybrid near-far field channels affect the detection performance. Simulation results validate the theoretical analysis and demonstrate the superior performance of the proposed approach compared with existing approaches.

**Index Terms**—Cell-free massive multiple-input multiple-output, distributed activity detection, grant-free random access, hybrid near-far field communications, machine-type communications.

## I. INTRODUCTION

With the rapid development of the Internet of Things (IoT), massive machine-type communications (mMTC) are expected to play a crucial role for the sixth-generation (6G) vision of ubiquitous connectivity [1]. To meet the stringent low-latency requirements, grant-free random access has been demonstrated as a promising solution compared to traditional grant-based schemes [2], [3].

Activity detection is a crucial task during the grant-free random access phase. Mathematically, current studies on activity detection can be broadly divided into two lines. In the first line of research, by exploiting the sporadic nature of mMTC, the compressed sensing (CS)-based method is proposed to solve the joint activity detection and channel estimation problem [4], [5]. Another line of research, known as the covariance-based approach, identifies active devices by leveraging the statistical properties of channels based on the covariance matrix without estimating the channels [6], [7]. Both theoretically and empirically, it has been demonstrated

that the covariance-based approach generally outperforms the CS-based approach [8].

Recently, cell-free massive multiple-input multiple-output (MIMO) has emerged as a key enabling technology to achieve the 6G vision of ubiquitous connectivity, where all access points (APs) are connected to a central processing unit (CPU) via fronthaul links for joint signal processing [9]. This architecture eliminates traditional cell boundaries, thereby overcoming inter-cell interference. Meanwhile, by deploying the large-scale antenna arrays at the APs, cell-free massive MIMO can achieve exceptionally high system capacity and enhanced spatial resolution [10].

On the other hand, as the array aperture enlarges, the boundary between the near-field and the far-field regions, characterized by the Rayleigh distance also expands [11]–[13]. Consequently, devices may be randomly distributed in either the near-field or the far-field region of each AP. Due to the fundamental difference of the electromagnetic wave propagation between the near-field and the far-field channels, the conventional assumption of the far-field propagation alone becomes impractical, necessitating the consideration of the hybrid near-far field communications. Furthermore, due to the hybrid near-far field channels, the received signals at each AP exhibit spatial correlations. Consequently, the rank-one update usually employed in the covariance-based method is not applicable anymore, rendering the algorithm design for activity detection mathematically intractable.

To overcome the above challenges, this paper proposes a practical hybrid near-far field system model for activity detection in cell-free massive MIMO. We derive the probability density function (PDF) of the received signals and establish a covariance-based formulation. Furthermore, to reduce the computational burden at the CPU, a distributed covariance-based activity detection algorithm is proposed to balance the computations across the network. Specifically, each AP performs local activity detection for the devices and then transmits the detection result to the CPU for further processing. In particular, a novel coordinate descent (CD) algorithm based on the Sherman-Morrison-Woodbury update with Taylor expansion is proposed to efficiently handle the local detection problem at each AP.

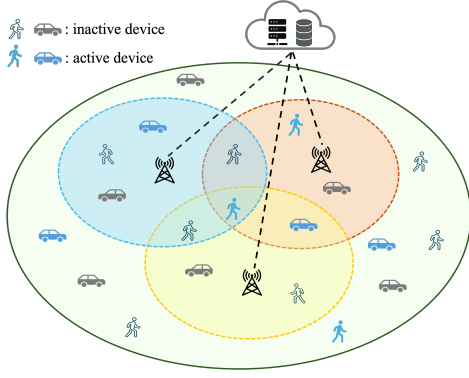


Fig. 1 Hybrid near-far field activity detection in cell-free massive MIMO.

Moreover, we theoretically reveal that the hybrid near-far field channels can improve the detection performance compared with the conventional far-field channels. Simulation results demonstrate that the proposed approach achieves better detection performance compared to existing methods, and also corroborates the theoretical analysis.

## II. SYSTEM MODEL AND PROBLEM FORMULATION

### A. System Model

As shown in Fig 1, consider an uplink cell-free massive MIMO system with  $M$  APs and  $N$  IoT devices. Each AP is equipped with a  $K$ -antenna uniform linear array with a half-wavelength space, and each IoT device utilizes a single antenna. All  $M$  APs communicate with a CPU through fronthaul links. The channels between the APs and the devices are assumed to undergo quasi-static block fading, which remains unchanged within each coherence block, but may vary across different blocks. Due to the boundary of the Rayleigh distance  $2D^2/\lambda_c$ , where  $D$  is the aperture of the antenna array, and  $\lambda_c$  is the wavelength of the central carrier, some devices are located in the near-field region of an AP if they are within its Rayleigh distance, and the remaining devices are located in its far-field region. For each AP  $m$ , let  $\mathcal{U}_m$  denote the subset containing  $N_{m,\text{near}}$  devices in the near-field region, and  $\mathcal{U}_m^c$  denote the complement set containing the remaining  $N - N_{m,\text{near}}$  devices in the far-field region. If device  $n$  is located in the far-field region of AP  $m$ , the uplink channel can be modeled as [10]:

$$\mathbf{h}_{m,n} \sim \mathcal{CN}(\mathbf{0}, g_{m,n} \mathbf{I}_K), \quad \forall n \in \mathcal{U}_m^c, \quad (1)$$

where  $g_{m,n}$  is the large-scale fading coefficient. If device  $n$  is located in the near-field region of AP  $m$ , its uplink channel consists of a deterministic light-of-sight (LoS) channel and a statistical multi-path non-light-of-sight (NLoS) channel induced by  $L_m$  scatterers [14]. Then, the near-field channel can be modeled as [15, Eq. (132)]:

$$\mathbf{h}_{m,n} = \underbrace{\beta_{m,n} \mathbf{b}_{m,n}(\mathbf{r}_{m,n})}_{\text{LoS}} + \underbrace{\sum_{\ell=1}^{L_m} \varphi_{m,\ell} \tilde{\beta}_{m,n,\ell} \mathbf{b}_{m,n}(\tilde{\mathbf{r}}_{m,\ell})}_{\text{NLoS}}, \quad \forall n \in \mathcal{U}_m, \quad (2)$$

where  $\beta_{m,n}$  and  $\tilde{\beta}_{m,n,\ell}$  denote the LoS and the NLoS channel gains, respectively,  $\varphi_{m,\ell} \sim \mathcal{CN}(0, \sigma_{m,\ell}^2)$  is the reflection coefficient of the  $\ell$ -th scatterer of AP  $m$  with variance  $\sigma_{m,\ell}^2$ ,  $[\mathbf{r}_{m,n}]_k$  is the distance between device  $n$  and the  $k$ -th antenna of AP  $m$ , and  $[\tilde{\mathbf{r}}_{m,\ell}]_k$  denotes the distance between scatter  $\ell$  and the  $k$ -th antenna of AP  $m$ . Furthermore,  $\mathbf{b}_{m,n}(\cdot)$  denotes the near-field array response. For instance, for the LoS channel, the array response is given by

$$\mathbf{b}_{m,n}(\mathbf{r}_{m,n}) = [e^{-j\frac{2\pi}{\lambda}([\mathbf{r}_{m,n}]_1 - r_{m,n,0})}, e^{-j\frac{2\pi}{\lambda}([\mathbf{r}_{m,n}]_2 - r_{m,n,0})}, \dots, e^{-j\frac{2\pi}{\lambda}([\mathbf{r}_{m,n}]_K - r_{m,n,0})}]^T, \quad (3)$$

where  $r_{m,n,0}$  is the distance between device  $n$  and the central element of AP  $m$ . Then, we can calculate the covariance matrix of  $\mathbf{h}_{m,n}$  as

$$\mathbf{R}_{m,n} = \sum_{\ell=1}^{L_m} \sigma_{m,\ell}^2 |\tilde{\beta}_{m,n,\ell}|^2 \mathbf{b}_{m,n}(\tilde{\mathbf{r}}_{m,\ell}) \mathbf{b}_{m,n}^H(\tilde{\mathbf{r}}_{m,\ell}), \quad \forall n \in \mathcal{U}_m. \quad (4)$$

On this basis, the near-field channel  $\mathbf{h}_{m,n}$  can be modeled as

$$\mathbf{h}_{m,n} \sim \mathcal{CN}(\beta_{m,n} \mathbf{b}_{m,n}(\mathbf{r}_{m,n}), \mathbf{R}_{m,n}), \quad \forall n \in \mathcal{U}_m. \quad (5)$$

To detect the device activity, each device  $n$  is pre-assigned a distinct signature sequence  $\mathbf{s}_n \in \mathbb{C}^L$ , where  $L$  represents the length of the signature sequence. Given the sporadic nature of mMTC, only a small fraction of the  $N$  devices remain active within each coherence block. Let  $a_n \in \{0, 1\}$  denote the binary variable for device  $n$  ( $a_n = 1$  denotes the active status). Then, the received signal at AP  $m$  can be written as

$$\mathbf{Y}_m = \sum_{n \in \mathcal{U}_m} a_n \mathbf{s}_n \mathbf{h}_{m,n}^T + \sum_{n \in \mathcal{U}_m^c} a_n \mathbf{s}_n \mathbf{h}_{m,n}^T + \mathbf{W}_m, \quad (6)$$

where  $\mathbf{W}_m \in \mathbb{C}^{L \times K}$  is the additive independent and identically distributed (i.i.d.) Gaussian noise at AP  $m$  with each entry following  $\mathcal{CN}(0, \zeta_m^2)$  and  $\zeta_m^2$  denoting the noise variance.

### B. Problem Formulation

Mathematically, the problem of activity detection is equivalent to determining each  $a_n \in \{0, 1\}$ . Notice that the channels and the noise are all complex Gaussian random variables, while  $\{\mathbf{s}_n\}_{n=1}^N$  and  $\{a_n\}_{n=1}^N$  can be viewed as deterministic. Consequently, the received signal  $\mathbf{Y}_m$  in (6) follows a complex Gaussian distribution as well. Given that the columns of  $\mathbf{Y}_m$  are not i.i.d. due to the near-field correlated channels, we analyze the joint distribution of all columns collectively. Thus, we consider its vectorized form  $\mathbf{y}_m = \text{vec}(\mathbf{Y}_m)$ , which can be written as

$$\mathbf{y}_m = \sum_{n \in \mathcal{U}_m} a_n \mathbf{h}_{m,n} \otimes \mathbf{s}_n + \sum_{n \in \mathcal{U}_m^c} a_n \mathbf{h}_{m,n} \otimes \mathbf{s}_n + \mathbf{w}_m, \quad (7)$$

where  $\otimes$  denotes the Kronecker product, and  $\mathbf{w}_m$  is the vectorized noise. Thus, we have  $\mathbf{y}_m \sim \mathcal{CN}(\bar{\mathbf{y}}_m, \mathbf{C}_m)$ , where

the mean and the covariance matrix are calculated based on (1) and (5), which are given by

$$\begin{aligned}\bar{\mathbf{y}}_m &= \sum_{n \in \mathcal{U}_m} a_n (\beta_{m,n} \mathbf{b}_{m,n}(\mathbf{r}_{m,n})) \otimes \mathbf{s}_n, \\ \mathbf{C}_m &= \sum_{n \in \mathcal{U}_m} a_n \mathbf{R}_{m,n} \otimes (\mathbf{s}_n \mathbf{s}_n^H) + \sum_{n \in \mathcal{U}_m^c} a_n g_{m,n} \mathbf{I}_K \otimes (\mathbf{s}_n \mathbf{s}_n^H) \\ &\quad + \varsigma_m^2 \mathbf{I}_{LK}.\end{aligned}\quad (8)$$

Then, the joint PDF of the received signals  $\{\mathbf{y}_m\}_{m=1}^M$  is given by

$$\begin{aligned}p(\{\mathbf{y}_m\}_{m=1}^M; \mathbf{a}) \\ = \prod_{m=1}^M \frac{1}{|\pi \mathbf{C}_m|} \exp(-(\mathbf{y}_m - \bar{\mathbf{y}}_m)^H \mathbf{C}_m^{-1} (\mathbf{y}_m - \bar{\mathbf{y}}_m)),\end{aligned}\quad (9)$$

where  $\mathbf{a} \triangleq [a_1, a_2, \dots, a_N]^T$  denotes the activity status vector. Our goal is to minimize the negative log-likelihood function  $-\log p(\{\mathbf{y}_m\}_{m=1}^M; \mathbf{a})$ , which is formulated as

$$\min_{\mathbf{a} \in [0,1]^N} \sum_{m=1}^M \{\log |\mathbf{C}_m| + (\mathbf{y}_m - \bar{\mathbf{y}}_m)^H \mathbf{C}_m^{-1} (\mathbf{y}_m - \bar{\mathbf{y}}_m)\}. \quad (10)$$

Once problem (10) is solved, the device activity is detected as  $\hat{a}_n = \mathbb{I}(a_n \geq \gamma)$ , where  $\mathbb{I}(\cdot)$  is an indicator function, and  $\gamma$  serves as a threshold within the range  $[0, 1]$  to balance the probability of missed detection (PM) and the probability of false alarm (PF) [10].

### III. DISTRIBUTED ACTIVITY DETECTION

In this section, we develop a distributed algorithm to tackle problem (10). Unlike the centralized method where the CPU handles all computations, the proposed distributed algorithm operates on both the APs and the CPU. Each AP conducts their local detection and then transmits the detection result to the CPU. Then, the CPU aggregates these results and distributes the combined information back to all APs to prepare for the subsequent iteration.

To enable distributed processing, we first reformulate problem (10) as an equivalent consensus form:

$$\min_{\{\boldsymbol{\theta}_m\}_{m=1}^M, \mathbf{a} \in [0,1]^N} \sum_{m=1}^M f_m(\boldsymbol{\theta}_m), \quad (11a)$$

$$\text{s.t. } \boldsymbol{\theta}_m = \mathbf{a}, \quad \forall m = 1, 2, \dots, M, \quad (11b)$$

where  $f_m(\boldsymbol{\theta}_m) = \log |\tilde{\mathbf{C}}_m| + (\mathbf{y}_m - \tilde{\mathbf{y}}_m)^H \tilde{\mathbf{C}}_m^{-1} (\mathbf{y}_m - \tilde{\mathbf{y}}_m)$ , and  $\tilde{\mathbf{C}}_m$  and  $\tilde{\mathbf{y}}_m$  follow the same structure as  $\mathbf{C}_m$  and  $\bar{\mathbf{y}}_m$  but with  $\boldsymbol{\theta}_m$  replacing  $\mathbf{a}$  in (8). Note that  $f_m(\cdot)$  only depends on the local calculation at the  $m$ -th AP, making it suitable for distributed optimization.

To solve problem (11) in a distributed manner, we construct its augmented Lagrangian function:

$$\begin{aligned}\mathcal{L}(\{\boldsymbol{\theta}_m\}_{m=1}^M, \mathbf{a}; \{\boldsymbol{\lambda}_m\}_{m=1}^M) \\ = \sum_{m=1}^M \left\{ f_m(\boldsymbol{\theta}_m) + \boldsymbol{\lambda}_m^T (\boldsymbol{\theta}_m - \mathbf{a}) + \frac{\mu}{2} \|\boldsymbol{\theta}_m - \mathbf{a}\|_2^2 \right\},\end{aligned}\quad (12)$$

where  $\boldsymbol{\lambda}_m \in \mathbb{R}^N$  is the dual variable associated with the consensus constraint  $\boldsymbol{\theta}_m = \mathbf{a}$ , and  $\mu > 0$  is a penalty parameter. We adopt the alternating direction method of multipliers framework by alternately updating  $\mathbf{a}$ ,  $\{\boldsymbol{\theta}_m\}_{m=1}^M$ , and  $\{\boldsymbol{\lambda}_m\}_{m=1}^M$ .

1) *Subproblem with respect to  $\{\boldsymbol{\theta}_m\}_{m=1}^M$* : At the  $i$ -th iteration, we decompose the problem with respect to  $\{\boldsymbol{\theta}_m\}_{m=1}^M$  into  $M$  parallel subproblems, with each processed by the corresponding AP and given by

$$\min_{\boldsymbol{\theta}_m} f_m(\boldsymbol{\theta}_m) + \left( \boldsymbol{\lambda}_m^{(i-1)} \right)^T (\boldsymbol{\theta}_m - \mathbf{a}^{(i-1)}) + \frac{\mu}{2} \|\boldsymbol{\theta}_m - \mathbf{a}^{(i-1)}\|_2^2. \quad (13)$$

This is a single-cell activity detection problem with additional linear and quadratic terms. Compared with the traditional far-field scenario, the dimension of the covariance matrix  $\tilde{\mathbf{C}}_m$  in problem (13) is  $LK \times LK$ , which is much larger than that in the far-field scenario, i.e.,  $L \times L$  [8]–[10]. Therefore, the complexity of updating and storing the matrix  $\tilde{\mathbf{C}}_m$  is much higher than that in the far-field scenario. Moreover, due to the existence of the channel correlation, the rank-one update in the existing covariance-based approach [6], [10], [16] is not applicable anymore, making problem (13) challenging to solve.

To tackle the above challenges, we propose a novel CD algorithm based on the Sherman-Morrison-Woodbury update with Taylor expansion. For notational simplicity, we first introduce several unified symbols. Let

$$\bar{\mathbf{h}}_{m,n} = \begin{cases} \beta_{m,n} \mathbf{b}_{m,n}(\mathbf{r}_{m,n}), & \text{if } n \in \mathcal{U}_m, \\ \mathbf{0}, & \text{if } n \in \mathcal{U}_m^c, \end{cases} \quad (14)$$

$$\Xi_{m,n} = \begin{cases} \mathbf{R}_{m,n}, & \text{if } n \in \mathcal{U}_m, \\ g_{m,n} \mathbf{I}_K, & \text{if } n \in \mathcal{U}_m^c. \end{cases} \quad (15)$$

Then, we can define a matrix  $\mathbf{X}_{m,n} = \Xi_{m,n}^{\frac{1}{2}} \otimes \mathbf{s}_n$  so that

$$\mathbf{X}_{m,n} \mathbf{X}_{m,n}^H = \Xi_{m,n} \otimes (\mathbf{s}_n \mathbf{s}_n^H). \quad (16)$$

Define  $\mathbf{e}_n \in \mathbb{R}^N$  as the standard basis vector whose  $n$ -th entry is 1 while all other entries are 0. For the  $n$ -th coordinate of  $\boldsymbol{\theta}_m$ , the update of  $\theta_{m,n}$  can be expressed as  $\theta_{m,n} + d$  with  $\{\theta_{m,n'}\}_{n'=1, n' \neq n}^N$  fixed, where  $d$  is determined by solving the following one-dimensional subproblem:

$$\begin{aligned}\min_{d \in [-\theta_{m,n}, 1 - \theta_{m,n}]} \log |\tilde{\mathbf{C}}_m + d \mathbf{X}_{m,n} \mathbf{X}_{m,n}^H| \\ + (\mathbf{y}_m - \tilde{\mathbf{y}}_m - d \bar{\mathbf{h}}_{m,n} \otimes \mathbf{s}_n)^H \left( \tilde{\mathbf{C}}_m + d \mathbf{X}_{m,n} \mathbf{X}_{m,n}^H \right)^{-1} \\ \times (\mathbf{y}_m - \tilde{\mathbf{y}}_m - d \bar{\mathbf{h}}_{m,n} \otimes \mathbf{s}_n) \\ + (\boldsymbol{\lambda}_m^{(i-1)})^T (\boldsymbol{\theta}_m + d \mathbf{e}_n - \mathbf{a}^{(i-1)}) + \frac{\mu}{2} \|\boldsymbol{\theta}_m + d \mathbf{e}_n - \mathbf{a}^{(i-1)}\|_2^2.\end{aligned}\quad (17)$$

According to the property of the determinant, we have

$$\begin{aligned}
& \log \left| \tilde{\mathbf{C}}_m + d \mathbf{X}_{m,n} \mathbf{X}_{m,n}^H \right| \\
&= \log \left| \mathbf{I}_{LK} + d \mathbf{X}_{m,n} \mathbf{X}_{m,n}^H \tilde{\mathbf{C}}_m^{-1} \right| + \log \left| \tilde{\mathbf{C}}_m \right| \\
&= \log \left| \mathbf{I}_{J_{m,n}} + d \mathbf{X}_{m,n}^H \tilde{\mathbf{C}}_m^{-1} \mathbf{X}_{m,n} \right| + \log \left| \tilde{\mathbf{C}}_m \right| \\
&\stackrel{(a)}{\approx} d \operatorname{tr} \left( \mathbf{X}_{m,n}^H \tilde{\mathbf{C}}_m^{-1} \mathbf{X}_{m,n} \right) + \log \left| \tilde{\mathbf{C}}_m \right|, \quad (18)
\end{aligned}$$

where  $J_{m,n} = \operatorname{rank}(\Xi_{m,n})$ , and (a) is derived from the first-order Taylor expansion to avoid the computational complexity in calculating the determinant. On the other hand, based on the Sherman-Morrison-Woodbury formula, we have

$$\begin{aligned}
& \left( \tilde{\mathbf{C}}_m + d \mathbf{X}_{m,n} \mathbf{X}_{m,n}^H \right)^{-1} \\
&= \tilde{\mathbf{C}}_m^{-1} - d \tilde{\mathbf{C}}_m^{-1} \mathbf{X}_{m,n} \\
&\quad \times \left( \mathbf{I}_{J_{m,n}} + d \mathbf{X}_{m,n}^H \tilde{\mathbf{C}}_m^{-1} \mathbf{X}_{m,n} \right)^{-1} \mathbf{X}_{m,n}^H \tilde{\mathbf{C}}_m^{-1} \\
&\stackrel{(b)}{\approx} \tilde{\mathbf{C}}_m^{-1} - d \tilde{\mathbf{C}}_m^{-1} \mathbf{X}_{m,n} \left( \mathbf{I}_{J_{m,n}} - d \mathbf{X}_{m,n}^H \tilde{\mathbf{C}}_m^{-1} \mathbf{X}_{m,n} \right) \\
&\quad \times \mathbf{X}_{m,n}^H \tilde{\mathbf{C}}_m^{-1}, \quad (19)
\end{aligned}$$

where (b) also applies the first-order Taylor expansion to avoid the computational complexity in repeatedly calculating the matrix inverse. Substituting the right-hand sides of (18) and (19) into (17), we obtain the CD update as shown in (20) at the top of the next page, where  $\lambda_{m,n}^{(i-1)}$  denotes the  $n$ -th entry of  $\boldsymbol{\lambda}_m^{(i-1)}$ . Setting the gradient of (20) to zero, the roots can be calculated by the cubic formula [17]. The optimal solution of problem (20) can be obtained by selecting the one with the smallest objective value among the roots. After sequentially updating  $\theta_{m,n}$  for all  $n$ , problem (20) can be efficiently solved to obtain  $\theta_m^{(i)}$  at each AP  $m$ .

2) *Updating the dual variables  $\{\boldsymbol{\lambda}_m\}_{m=1}^M$* : After updating  $\{\theta_m\}_{m=1}^M$ ,  $\{\boldsymbol{\lambda}_m\}_{m=1}^M$  are updated by a dual ascent step:

$$\boldsymbol{\lambda}_m^{(i)} = \boldsymbol{\lambda}_m^{(i-1)} + \mu \left( \theta_m^{(i)} - \mathbf{a}^{(i-1)} \right), \forall m = 1, 2, \dots, M. \quad (21)$$

3) *Subproblem with respect to  $\mathbf{a}$* : We decompose the problem with respect to  $\mathbf{a}$  into  $N$  parallel subproblems, with each written as

$$\min_{a_n \in [0,1]} \sum_{m=1}^M \left\{ \lambda_{m,n}^{(i)} \left( \theta_{m,n}^{(i)} - a_n \right) + \frac{\mu}{2} \left( \theta_{m,n}^{(i)} - a_n \right)^2 \right\}, \quad (22)$$

where  $\theta_{m,n}^{(i)}$  denotes the  $n$ -th entry of  $\theta_m^{(i)}$ . Problem (22) is a one-dimensional convex quadratic problem, and hence its optimal solution can be derived in a closed form:

$$a_n^{(i)} = \Pi_{[0,1]} \left( \delta_n^{(i)} \right), \quad \forall n = 1, 2, \dots, N, \quad (23)$$

where  $\delta_n^{(i)} = \sum_{m=1}^M \left( \mu \theta_{m,n}^{(i)} + \lambda_{m,n}^{(i)} \right) / (M\mu)$ , and  $\Pi_{[0,1]}(\cdot)$  is the projection operation onto  $[0, 1]$ .

---

**Algorithm 1** Proposed Distributed Algorithm for Solving Problem (11)

---

- 1: **Initialize:**  $\boldsymbol{\theta}_m^{(0)}, \boldsymbol{\lambda}_m^{(0)}, \forall m = 1, 2, \dots, M$ , and  $\mathbf{a}^{(0)}$  using (23);
  - 2: **repeat** ( $i = 1, 2, \dots$ )
  - 3:   The CPU broadcasts  $\mathbf{a}^{(i-1)}$  to each AP  $m$ ,  $\forall m = 1, 2, \dots, M$ ;
  - 4:   Each AP  $m$  updates  $\boldsymbol{\theta}_m^{(i)}$  by sequentially solving problem (20) with respect to all coordinates,  $\forall m = 1, 2, \dots, M$ ;
  - 5:   Each AP  $m$  updates  $\boldsymbol{\lambda}_m^{(i)}$  by a dual ascent step (21),  $\forall m = 1, 2, \dots, M$ ;
  - 6:   Each AP  $m$  sends  $\mu \boldsymbol{\theta}_m^{(i)} + \boldsymbol{\lambda}_m^{(i)}$  to the CPU,  $\forall m = 1, 2, \dots, M$ ;
  - 7:   The CPU updates  $\mathbf{a}^{(i)}$  with (23);
  - 8: **until** convergence
- 

Through iterative updates of both primal and dual variables, we present a distributed algorithm to solve problem (11), with the complete procedure outlined in Algorithm 1. Although problem (11) is nonconvex, the following theorem demonstrates that Algorithm 1 can converge to a stationary point. We omit the proof due to space limitations.

**Theorem 1.** *Let  $L_m$  denote the Lipschitz constant of  $\nabla f_m(\boldsymbol{\theta}_m)$  and  $\rho = \bar{\rho}_2 + \bar{\rho}_3 + \bar{\rho}_4$  be a constant, where  $\bar{\rho}_2, \bar{\rho}_3$ , and  $\bar{\rho}_4$  are the upper bounds of  $\rho_2(\boldsymbol{\theta}_m), \rho_3(\boldsymbol{\theta}_m)$ , and  $\rho_4(\boldsymbol{\theta}_m)$  in (20), respectively. When  $\mu > \max\{2L_m, L_m + \rho\}$ , the solution sequence  $\{\mathbf{a}^{(i)}\}$  generated by Algorithm 1 converges to a stationary point of problem (11).*

#### IV. PERFORMANCE ANALYSIS

In this section, we analyze how the hybrid near-far field channels affect the detection performance. To achieve good detection performance, the true activity indicator vector  $\mathbf{a}^\circ$  should be uniquely identifiable. Specifically, there should not exist another vector  $\tilde{\mathbf{a}} \neq \mathbf{a}^\circ$  that yields the same PDF, i.e.,  $p(\{\mathbf{y}_m\}_{m=1}^M; \tilde{\mathbf{a}}) = p(\{\mathbf{y}_m\}_{m=1}^M; \mathbf{a}^\circ)$ . Given that both distributions are multivariate Gaussian, this equivalence requires identical means and covariance matrices. According to the second equation of (8), when the covariance matrices are identical, we have

$$\sum_{n \in \mathcal{U}_m} (\tilde{a}_n - a_n^\circ) \mathbf{R}_{m,n} \otimes (\mathbf{s}_n \mathbf{s}_n^H) + \sum_{n \in \mathcal{U}_m^c} (\tilde{a}_n - a_n^\circ) g_{m,n} \mathbf{I}_K \otimes (\mathbf{s}_n \mathbf{s}_n^H) = \mathbf{O}, \quad (24)$$

where  $\tilde{a}_n$  and  $a_n^\circ$  denote the  $n$ -th entry of  $\tilde{\mathbf{a}}$  and  $\mathbf{a}^\circ$ , respectively, and  $\mathbf{O}$  denotes the zero matrix. After vectorization and using the definition of  $\mathbf{X}_{m,n}$  in (16), we have

$$\boldsymbol{\Psi}_m \boldsymbol{\xi} = \mathbf{0}, \quad (25)$$

where  $\boldsymbol{\xi} = \tilde{\mathbf{a}} - \mathbf{a}^\circ$  and

$$\boldsymbol{\Psi}_m = [\operatorname{vec}(\mathbf{X}_{m,1} \mathbf{X}_{m,1}^H), \operatorname{vec}(\mathbf{X}_{m,2} \mathbf{X}_{m,2}^H), \dots, \operatorname{vec}(\mathbf{X}_{m,N} \mathbf{X}_{m,N}^H)]. \quad (26)$$

$$\begin{aligned}
& \min_{d \in [-\theta_{m,n}, 1-\theta_{m,n}]} d\rho_1(\boldsymbol{\theta}_m) + d^2\rho_2(\boldsymbol{\theta}_m) + d^3\rho_3(\boldsymbol{\theta}_m) + d^4\rho_4(\boldsymbol{\theta}_m) \\
& \rho_1(\boldsymbol{\theta}_m) = \text{tr} \left( \mathbf{X}_{m,n}^H \tilde{\mathbf{C}}_m^{-1} \mathbf{X}_{m,n} \right) - 2 \text{Re} \left( (\mathbf{y}_m - \tilde{\mathbf{y}}_m)^H \tilde{\mathbf{C}}_m^{-1} (\bar{\mathbf{h}}_{m,n} \otimes \mathbf{s}_n) \right) \\
& \quad - (\mathbf{y}_m - \tilde{\mathbf{y}}_m)^H \tilde{\mathbf{C}}_m^{-1} \mathbf{X}_{m,n} \mathbf{X}_{m,n}^H \tilde{\mathbf{C}}_m^{-1} (\mathbf{y}_m - \tilde{\mathbf{y}}_m) + \lambda_{m,n}^{(i-1)} + \mu \left( \theta_{m,n} - a_n^{(i-1)} \right), \\
& \rho_2(\boldsymbol{\theta}_m) = (\bar{\mathbf{h}}_{m,n} \otimes \mathbf{s}_n)^H \tilde{\mathbf{C}}_m^{-1} (\bar{\mathbf{h}}_{m,n} \otimes \mathbf{s}_n) + 2 \text{Re} \left( (\mathbf{y}_m - \tilde{\mathbf{y}}_m)^H \tilde{\mathbf{C}}_m^{-1} \mathbf{X}_{m,n} \mathbf{X}_{m,n}^H \tilde{\mathbf{C}}_m^{-1} (\bar{\mathbf{h}}_{m,n} \otimes \mathbf{s}_n) \right) \\
& \quad + (\mathbf{y}_m - \tilde{\mathbf{y}}_m)^H \tilde{\mathbf{C}}_m^{-1} \mathbf{X}_{m,n} \mathbf{X}_{m,n}^H \tilde{\mathbf{C}}_m^{-1} \mathbf{X}_{m,n} \mathbf{X}_{m,n}^H \tilde{\mathbf{C}}_m^{-1} (\mathbf{y}_m - \tilde{\mathbf{y}}_m) + \frac{\mu}{2}, \\
& \rho_3(\boldsymbol{\theta}_m) = -2 \text{Re} \left( (\mathbf{y}_m - \tilde{\mathbf{y}}_m)^H \tilde{\mathbf{C}}_m^{-1} \mathbf{X}_{m,n} \mathbf{X}_{m,n}^H \tilde{\mathbf{C}}_m^{-1} \mathbf{X}_{m,n} \mathbf{X}_{m,n}^H \tilde{\mathbf{C}}_m^{-1} (\bar{\mathbf{h}}_{m,n} \otimes \mathbf{s}_n) \right) \\
& \quad - (\bar{\mathbf{h}}_{m,n} \otimes \mathbf{s}_n)^H \tilde{\mathbf{C}}_m^{-1} \mathbf{X}_{m,n} \mathbf{X}_{m,n}^H \tilde{\mathbf{C}}_m^{-1} (\bar{\mathbf{h}}_{m,n} \otimes \mathbf{s}_n), \\
& \rho_4(\boldsymbol{\theta}_m) = (\bar{\mathbf{h}}_{m,n} \otimes \mathbf{s}_n)^H \tilde{\mathbf{C}}_m^{-1} \mathbf{X}_{m,n} \mathbf{X}_{m,n}^H \tilde{\mathbf{C}}_m^{-1} \mathbf{X}_{m,n} \mathbf{X}_{m,n}^H \tilde{\mathbf{C}}_m^{-1} (\bar{\mathbf{h}}_{m,n} \otimes \mathbf{s}_n). \tag{20}
\end{aligned}$$

Let

$$\mathcal{V} = \{\boldsymbol{\xi} \in \mathbb{R}^N | \boldsymbol{\Psi}_m \boldsymbol{\xi} = \mathbf{0}, \boldsymbol{\xi} \neq \mathbf{0}, \forall m = 1, 2, \dots, M\}, \tag{27}$$

$$\mathcal{D} = \{\boldsymbol{\xi} \in \mathbb{R}^N | \xi_n \geq 0 \text{ if } a_n^\circ = 0, \xi_n \leq 0 \text{ if } a_n^\circ = 1\}, \tag{28}$$

where (27) defines the solution set containing any other  $\tilde{\mathbf{a}} \neq \mathbf{a}^\circ$  that yields the same covariance matrix, while (28) defines the feasible set of problem (10). Consequently, the identifiability of  $\mathbf{a}^\circ$  requires at least  $\mathcal{V} \cap \mathcal{D} = \emptyset$ . From (27), we can observe that if the columns of  $\boldsymbol{\Psi}_m$  are closer to orthogonality, then the condition  $\mathcal{V} \cap \mathcal{D} = \emptyset$  is more likely to hold, which ensures better detection performance. The following proposition demonstrates that the columns of  $\boldsymbol{\Psi}_m$  in the hybrid near-far field channels are closer to orthogonality than those of the far-field channels.

**Proposition 1.** *For any two devices  $n$  and  $n'$ , the columns of  $\boldsymbol{\Psi}_m$  in the hybrid near-far field channels are closer to orthogonality in the sense that their cosine similarity is upper bounded by that of the far-field channels:*

$$\frac{(\boldsymbol{\psi}_{m,n})^H \boldsymbol{\psi}_{m,n'}}{\|\boldsymbol{\psi}_{m,n}\|_2 \|\boldsymbol{\psi}_{m,n'}\|_2} \leq \left( \frac{|\mathbf{s}_n^H \mathbf{s}_{n'}|}{\|\mathbf{s}_n\|_2 \|\mathbf{s}_{n'}\|_2} \right)^2, \tag{29}$$

where  $\boldsymbol{\psi}_{m,n}$  is the  $n$ -th column of  $\boldsymbol{\Psi}_m$ , and the equality holds if and only if  $\boldsymbol{\Xi}_{m,n} = c\boldsymbol{\Xi}_{m,n'}$  for some constant  $c$ .

*Proof.* Please see Appendix A.  $\square$

The above analysis demonstrates that the hybrid near-far field channels can effectively improve the detection performance as compared to the conventional far-field channels.

## V. SIMULATION RESULTS

In this section, we validate the performance of the proposed method through simulations in terms of the PM and the PF [10]. We consider a  $200 \times 200$  square meters area, i.e.,  $[-100, 100] \times [-100, 100]$ , with wrap-around at the boundary. There are  $N = 100$  IoT devices uniformly distributed in this square area, where the ratio of the active devices is 0.1. The signature sequence of each device  $\mathbf{s}_n$  is generated randomly and uniformly from the discrete set  $\left\{ \pm \frac{\sqrt{2}}{2} \pm j \frac{\sqrt{2}}{2} \right\}^L$  [16].

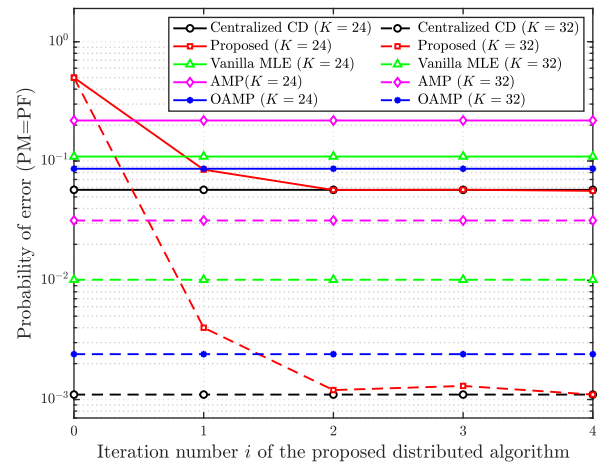
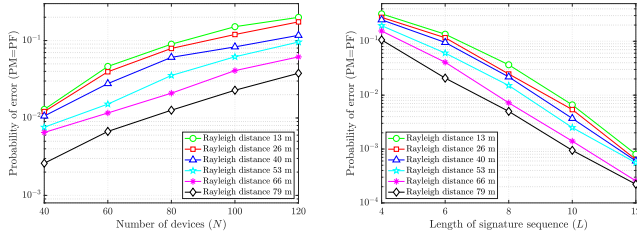


Fig. 2 Probability of error versus iteration number.

The number of the APs is set to  $M = 3$ , which are located at  $(40, 0)$ ,  $(-20, 20\sqrt{3})$ , and  $(-20, -20\sqrt{3})$ , respectively. The channel coefficients  $g_{m,n}$ ,  $\beta_{m,n}^2$ , and  $\tilde{\beta}_{m,n,\ell}^2$  follow the path-loss model, which is given by  $128.1 + 37.6 \log_{10}(\tau)$ , where  $\tau$  is the corresponding distance in km, the number of scatters at each AP is set to  $L_m = 8$ , and the variance of the reflection coefficient of each scatter is set to  $\sigma_{m,\ell}^2 = 1$ . The background noise power is set as  $-99$  dBm.

We compare the performance of the proposed distributed algorithm with the following benchmarks: Centralized CD [17], AMP [18], OAMP [19], and Vanilla MLE [20]. The probability of error when  $\text{PM} = \text{PF}$  is shown in Fig. 2, where  $L = 6$ ,  $K = 24$  or  $32$ , and  $D = (K - 1)\lambda_c/2$  with  $\lambda_c = 0.2$  m. We can see that the proposed distributed Algorithm 1 achieves a fast convergence speed within only 2 iterations, and the increased number of the antennas can improve the detection performance of all methods. Moreover, since the proposed algorithm leverages the problem formulation (10) based on an accurate hybrid-field channel model (8), it outperforms the exiting centralized approaches, including AMP, OAMP, and Vanilla MLE. Finally, as a distributed algorithm, the



(a) Probability of error versus  $N$  when  $L = 6$ . (b) Probability of error versus  $L$  when  $N = 100$ .

Fig. 3 Performance comparison across different Rayleigh distances.

proposed Algorithm 1 can achieve comparable performance to Centralized CD.

Figure 3 illustrates the detection performance across different Rayleigh distances, where  $K = 24$ , and  $D = (K - 1)\lambda_c/2$  with  $\lambda_c = 0.05$  m, 0.1 m, 0.15 m, 0.20, 0.25, and 0.3 m, which correspond to the Rayleigh distances of 13 m, 26 m, 40 m, 53 m, 66 m, and 79 m, respectively. It can be observed that a longer Rayleigh distance, which incorporates more near-field channels, leads to better detection performance under different device numbers and different lengths of signature sequences, verifying the theoretical analysis in Proposition 1.

## VI. CONCLUSION

This paper investigated the hybrid near-far field activity detection in cell-free massive MIMO and established a covariance-based formulation. Then, a distributed activity detection algorithm was proposed to alleviate the computational burden at the CPU. The theoretical analysis demonstrated that the hybrid near-far field channels can improve the detection performance compared with the conventional far-field channels. Simulation results corroborated the theoretical analysis and demonstrated that the proposed distributed approach achieves superior detection performance compared to the existing methods.

## APPENDIX A PROOF OF PROPOSITION 1

For devices  $n$  and  $n'$ , we have

$$\begin{aligned} \frac{(\psi_{m,n})^H \psi_{m,n'}}{\|\psi_{m,n}\|_2 \|\psi_{m,n'}\|_2} &= \frac{\text{vec}(\mathbf{X}_{m,n} \mathbf{X}_{m,n})^H \text{vec}(\mathbf{X}_{m,n'} \mathbf{X}_{m,n'})}{\|\text{vec}(\mathbf{X}_{m,n} \mathbf{X}_{m,n})\|_2 \|\text{vec}(\mathbf{X}_{m,n'} \mathbf{X}_{m,n'})\|_2} \\ &= \frac{\text{tr}(\mathbf{\Xi}_{m,n} \mathbf{\Xi}_{m,n'})}{\|\mathbf{\Xi}_{m,n}\|_F \|\mathbf{\Xi}_{m,n'}\|_F} \times \left( \frac{|\mathbf{s}_n^H \mathbf{s}_{n'}|}{\|\mathbf{s}_n\|_2 \|\mathbf{s}_{n'}\|_2} \right)^2 \\ &\stackrel{(a)}{\leq} \left( \frac{|\mathbf{s}_n^H \mathbf{s}_{n'}|}{\|\mathbf{s}_n\|_2 \|\mathbf{s}_{n'}\|_2} \right)^2, \end{aligned} \quad (30)$$

where (a) follows from the Cauchy-Schwartz inequality with the equality holding if and only if  $\mathbf{\Xi}_{m,n} = c\mathbf{\Xi}_{m,n'}$  for some constant  $c$ . The right-hand side of (30) is the cosine similarity of the far-field channels, which can be verified by substituting  $\mathbf{\Xi}_{m,n} = g_{m,n} \mathbf{I}_K$  and  $\mathbf{\Xi}_{m,n'} = g_{m,n'} \mathbf{I}_K$  into the left-hand side of (30).

## REFERENCES

- [1] Y.-F. Liu, T.-H. Chang, M. Hong, Z. Wu, A. M.-C. So, E. A. Jorswieck, and W. Yu, "A survey of recent advances in optimization methods for wireless communications," *IEEE J. Sel. Areas Commun.*, vol. 42, no. 11, pp. 2992–3031, 2024.
- [2] M. B. Shahab, R. Abbas, M. Shirvanimoghaddam, and S. J. Johnson, "Grant-free non-orthogonal multiple access for IoT: A survey," *IEEE Commun. Surveys Tuts.*, vol. 22, no. 3, pp. 1805–1838, 2020.
- [3] Y. Li, Z. Chen, Y. Wang, C. Yang, B. Ai, and Y.-C. Wu, "Heterogeneous transformer: A scale adaptable neural network architecture for device activity detection," *IEEE Trans. Wireless Commun.*, vol. 22, no. 5, pp. 3432–3446, 2023.
- [4] Y. Li, M. Xia, and Y.-C. Wu, "Activity detection for massive connectivity under frequency offsets via first-order algorithms," *IEEE Trans. Wireless Commun.*, vol. 18, no. 3, pp. 1988–2002, 2019.
- [5] Z. Gao, M. Ke, Y. Mei, L. Qiao, S. Chen, D. W. K. Ng, and H. V. Poor, "Compressive-sensing-based grant-free massive access for 6G massive communication," *IEEE IoT J.*, vol. 11, no. 5, pp. 7411–7435, 2023.
- [6] Y. Li, Q. Lin, Y.-F. Liu, B. Ai, and Y.-C. Wu, "Asynchronous activity detection for cell-free massive MIMO: From centralized to distributed algorithms," *IEEE Trans. Wireless Commun.*, vol. 22, no. 4, pp. 2477–2492, 2022.
- [7] Q. Lin, Y. Li, Y.-C. Wu, and R. Zhang, "Intelligent reflecting surface aided activity detection for massive access: Performance analysis and learning approach," *IEEE Trans. Wireless Commun.*, vol. 23, no. 11, pp. 16 935–16 949, 2024.
- [8] Z. Chen, F. Söhrabi, Y.-F. Liu, and W. Yu, "Phase transition analysis for covariance-based massive random access with massive MIMO," *IEEE Trans. Inf. Theory*, vol. 68, no. 3, pp. 1696–1715, 2021.
- [9] Q. Lin, Y. Li, W.-B. Kou, T.-H. Chang, and Y.-C. Wu, "Communication-efficient activity detection for cell-free massive MIMO: An augmented model-driven end-to-end learning framework," *IEEE Trans. Wireless Commun.*, vol. 23, no. 10, pp. 12 888–12 903, 2024.
- [10] U. K. Ganesan, E. Björnson, and E. G. Larsson, "Clustering-based activity detection algorithms for grant-free random access in cell-free massive MIMO," *IEEE Trans. Commun.*, vol. 69, no. 11, pp. 7520–7530, 2021.
- [11] H. Lu, Y. Zeng, C. You, Y. Han, J. Zhang, Z. Wang, Z. Dong, S. Jin, C.-X. Wang, T. Jiang, X. You, and R. Zhang, "A tutorial on near-field XL-MIMO communications toward 6G," *IEEE Commun. Surveys Tuts.*, vol. 26, no. 4, pp. 2213–2257, 2024.
- [12] M. Cui, Z. Wu, Y. Lu, X. Wei, and L. Dai, "Near-field MIMO communications for 6G: Fundamentals, challenges, potentials, and future directions," *IEEE Commun. Mag.*, vol. 61, no. 1, pp. 40–46, 2023.
- [13] Z. Wang, J. Zhang, H. Du, D. Niyato, S. Cui, B. Ai, M. Debbah, K. B. Letaief, and H. V. Poor, "A tutorial on extremely large-scale MIMO for 6G: Fundamentals, signal processing, and applications," *IEEE Commun. Surveys Tuts.*, vol. 26, no. 3, pp. 1560–1605, 2024.
- [14] Z. Wang, X. Mu, and Y. Liu, "Beamfocusing optimization for near-field wideband multi-user communications," *IEEE Trans. Commun.*, vol. 73, no. 1, pp. 555–572, 2025.
- [15] Y. Liu, Z. Wang, J. Xu, C. Ouyang, X. Mu, and R. Schober, "Near-field communications: A tutorial review," *IEEE Open J. Commun. Soc.*, vol. 4, pp. 1999–2049, 2023.
- [16] Z. Wang, Y.-F. Liu, Z. Wang, and W. Yu, "Covariance-based activity detection in cooperative multi-cell massive MIMO: Scaling law and efficient algorithms," *IEEE Trans. Inf. Theory*, vol. 70, no. 12, pp. 8770–8790, 2024.
- [17] Z. Wang, Y. Li, Y.-F. Liu, and J. Ma, "Covariance-based device activity detection with massive MIMO for near-field correlated channels," *arXiv:2411.05492*, 2024.
- [18] H. Djelouat, L. Marata, M. Leinonen, H. Alves, and M. Juntti, "User activity detection and channel estimation of spatially correlated channels via AMP in massive MTC," in *Proc. 55th Asilomar Conf. Signals Syst. Comput.*, 2021.
- [19] Y. Cheng, L. Liu, and L. Ping, "Orthogonal AMP for massive access in channels with spatial and temporal correlations," *IEEE J. Sel. Areas in Commun.*, vol. 39, no. 3, pp. 726–740, 2020.
- [20] W. Liu, Y. Cui, F. Yang, L. Ding, and J. Sun, "MLE-based device activity detection under Rician fading for massive grant-free access with perfect and imperfect synchronization," *IEEE Trans. Wireless Commun.*, vol. 23, no. 8, pp. 8787–8804, 2024.